Research Article | Vol. 31, No. 11 / 22 May 2023 / Optics Express 18567

Optics EXPRESS

Improvement of optical properties of InGaN-based red multiple quantum wells

XIN HOU,[1] TAO YANG,[1] SHAO-SHENG FAN,[1] HUAN XU,[1] DAISUKE IIDA,[2] YUE-JUN LIU,[3] YANG MEI,[1] GUO-EN WENG,[3] SHAO-QIANG CHEN,[3] BAO-PING ZHANG,[1,*] AND KAZUHIRO OHKAWA[1,2]

[1] *Laboratory of Micro/Nano-Optoelectronics, Department of Microelectronics and Integrated Circuits, Xiamen University, Xiamen 361005, China*

[2] *Computer, Electrical and Mathematical Sciences and Engineering (CEMSE) Division, King Abdullah University of Science and Technology (KAUST), Thuwal 23955-6900, Saudi Arabia*

[3] *State Key Laboratory of Precision Spectroscopy, Department of Electronic Engineering, East China Normal University, Shanghai 200241, China*

[*] *bzhang@xmu.edu.cn*

Abstract: The realization of red-emitting InGaN quantum well (QW) is a hot issue in current nitride semiconductor research. It has been shown that using a low-Indium (In)-content pre-well layer is an effective method to improve the crystal quality of red QWs. On the other hand, keeping uniform composition distribution at higher In content in red QWs is an urgent problem to be solved. In this work, the optical properties of blue pre-QW and red QWs with different well width and growth conditions are investigated by photoluminescence (PL). The results prove that the higher-In-content blue pre-QW is beneficial to effectively relieve the residual stress. Meanwhile, higher growth temperature and growth rate can improve the uniformity of In content and the crystal quality of red QWs, enhancing the PL emission intensity. Possible physical process of stress evolution and the model of In fluctuation in the subsequent red QW are discussed. This study provides a useful reference for the development of InGaN-based red emission materials and devices.

1. Introduction

III-nitride materials have attracted much attention due to the excellent performance such as wavelength tunability, high efficiency, high power, environmentally friendly character, etc. These properties make it widely used in solid-state lighting and displays. In the past few decades, InGaN-based blue and green light-emitting diodes (LEDs) have achieved great success based on the rapid development of InGaN materials. The maximum external quantum efficiencies (EQEs) of LEDs exceed 80% and 50%, respectively [1,2]. In recent years, the red-emitting materials and devices based on InGaN are attracting increasing attention. Presently, red LEDs based on aluminum indium gallium phosphide (AlInGaP) materials are of high efficiency and well-established, achieving a high EQE of over 60% [3]. But their thermal stability is poor, and their quantum efficiency drops fast as the temperature rises. In comparison, InGaN material offers superior thermal stability, mechanical and chemical capabilities, and is environmentally friendly [4]. Therefore, achieving high-efficiency red emission becomes particularly important for realizing three primary colors (RGB) through III-nitride materials.

Due to the high In content, the EQEs of even the state-of-the-art InGaN-based red LEDs are still less than that of typical blue and green LEDs. The major challenge in realizing high-efficiency red InGaN-based LEDs is the poor crystal quality. This is caused firstly by a low-temperature growth. Secondly, the red QWs with high In content are easily affected by the large lattice mismatch, leading to strong quantum-confined Stark effect (QCSE), large strain and In fluctuation

#488681 https://doi.org/10.1364/OE.488681
Journal © 2023 Received 24 Feb 2023; revised 7 May 2023; accepted 8 May 2023; published 18 May 2023

Optics EXPRESS

[5–8]. These issues result in a large peak-wavelength shift, a low internal quantum efficiency (IQE), and a large full width at half maximum (FWHM) of the red emission peak. In order to solve these problems, many research groups have adopted various growth strategies, such as InGaNOS pseudo-substrate [9], nano-porous GaN [10], strain relaxed InGaN buffer layer [11], strain compensating barrier layers [12], hybrid QW structures [13] and thick GaN template [14] etc. Through these methods, both the incorporation of In and the growth temperature were increased for red QWs. In 2021, Chan et al. fabricated the 633-nm InGaN-based red LEDs with a high growth temperature of 870 °C on a relaxed InGaN/GaN superlattice buffer [15]. In 2022, Iida et al. fabricated a 621-nm-wavelength InGaN-based LEDs using a single red quantum well as the active layer. By adopting a thick underlying n-GaN layer and a lower-In-content blue pre-single quantum well, they reduced the in-place stress and improved crystal quality of the InGaN active region, and achieved an EQE of 4.3% [16]. In 2022, by using blue InGaN single-QW and red InGaN double-QWs as active regions, Huang et al. achieved that the maximum value of EQE, 5.02%-6.71% [17].

Although the EQE of red QW is gradually improving, its optical properties and carrier dynamics still need to be studied and elucidated. We previous reported that the thick n-GaN underlayer is beneficial to enhance In content in red QW [18]. Meanwhile, increasing the uniformity of In composition and decreasing defects are the key challenges for achieving high-efficiency red emission. In this work, it is demonstrated that the blue pre-QW with higher In content can effectively relieve the residual stress coming from the underlayers. In addition, by proper growth conditions, the uniformity of In content and the crystal quality of the red QW are improved, and the IQE is enhanced. Using PL and time-resolved photoluminescence (TRPL) analyses, we investigated the intrinsic reason and carrier recombination mechanism why the red QWs with 3.5-nm well width possesses a stronger PL intensity and a narrower FWHM. A model is proposed to explain the emission mechanism of two different samples. The results may provide a guideline for the development of high-efficiency long-wavelength optoelectronic devices based on nitride semiconductors.

2. Sample structures and experiments

Figure 1 shows the cross-sectional schematic of two red MQWs wafers with different well thicknesses. One 2 nm single blue QW and two red QWs made up the InGaN MQWs. GaN(2 nm)/$Al_{0.13}Ga_{0.87}N$(18 nm)/ GaN(3 nm) barrier layers can well restrict carriers and play a role of stress compensation in QWs. It is well known that inserting a low-indium-content pre-well before growing high-indium-content InGaN on GaN will help to relax the strain and improve indium incorporation [14]. The well widths of red QWs are 2.5 and 3.5 nm for Sample 1 and Sample 2, respectively. Compared with Sample 1, the growth conditions were changed in Sample 2. Firstly, the growth temperature of blue pre-QW in sample 2 was reduced by 7 °C. And the growth rate of $Al_{0.13}Ga_{0.87}N$ of Sample 2 was reduced 25%. Secondly, for the red DQWs, the growth temperature was increased by 20 °C and the growth rate was doubled for Sample 2 [19]. The detail comparisons in growth conditions of two samples are shown in Table. 1.

Temperature-dependent PL measurements were performed at temperatures of 4-300 K. The excitation source was a 405 nm (5 ns, 20 Hz) pulsed laser. The laser spot diameter on the sample was 160 µm. Samples were mounted in a closed-circuit helium cryostat. A Princeton Instruments Model ACTONSpectrapro-3000i monochromator supplied the dispersion of the PL signal from the samples. On the other hand, TRPL measurements were performed at room temperature (RT). A 400 nm pulse laser was used as the excitation source, which was generated by frequency doubling a Ti:sapphire femtosecond (fs) pulse laser operating at 800 nm (35 fs, 1 kHz, Model Verdi G8, Coherent, America). The spot diameter of the laser is 50 µm. All the TRPL measurements were carried out by a home-built confocal µ-PL system at RT. TRPL spectra

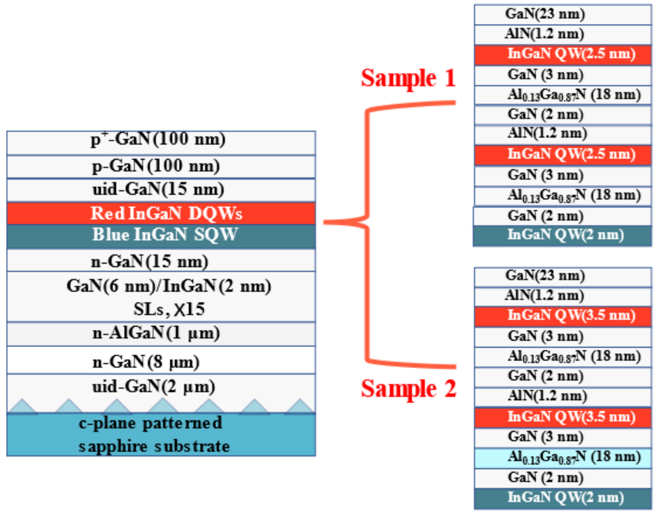

Fig. 1. Cross-sectional schematic of red InGaN-based LED structures: red QWs of Sample 1 with 2.5-nm well and that of Sample 2 with 3.5-nm well.

Table 1. The comparison in growth conditions of two samples

Structure	Sample 2 (compared with sample 1)
$Al_{0.13}Ga_{0.87}N$ (barrier)	Growth rate was reduced by 25%.
Blue QW (pre-well layer)	Growth temperature was reduced 7 °C.
Red QWs (active layers)	Wider well width (3.5 nm)
	Growth temperature was increased 20 °C.
	Growth rate was increased by 2 times.

were detected by a streak-camera system (C10910, Hamamatsu, Japan) with a temporal resolution of about 10 ps. TRPL measurements were carried out similarly as described in Ref. [20].

3. Experimental results and discussion

Firstly, the excitation-energy-dependent PL for two samples were measured at 4 K. The results indicate both samples have two emission peaks (blue peak and red peak). As our previous reports [18,21], the blue peak and red peak originated from the blue pre-QW and the red QWs, respectively. The normalized PL spectra of blue peak with different excitation energies for two samples at 4 K are shown in Fig. 2 (a) and (b), respectively. The longer emission wavelength of Sample 2 indicates a higher In composition in the pre-QW because of the lower growth temperature. With increasing excitation energy, the blue pre-QW emission of both samples exhibit blue-shift, caused by two possible effects: screening of QCSE and band filing. Sample 1 shows a severe broadening on the higher energy (shorter wavelength) side, showing that band filling effect is dominant. On the other hand, Sample 2 exhibited a obvious blue shift in the whole spectrum, showing that the screening of QCSE is dominant. Figure 2(c) and (d) show the dependence of emission energy and FWHM for the two samples. It can be seen that FWHM of Sample 2 is narrower (~12 nm) than Sample 1(>18 nm), indicating relatively homogeneous In distribution of pre-QW in Sample 2 while more In fluctuation in Sample 1 [18]. Moreover, the decreasing FWHM of Sample 2 and increasing peak energy at lower excitation energies are another evidence of screening QCSE effect as shown in Fig. 2 (d). The pre-QW of Sample 2 presents QCSE due to the higher In content and the less In fluctuation than that of Sample 1. The less fluctuation of In composition in Sample 2 is attributed to the lower growth rate (longer growth time) of the $Al_{0.13}Ga_{0.87}N$ barrier (decreased by 1/4). Longer growth time induces an annealing effect on the pre-QW, which is beneficial for In homogeneity and then improve the radiation recombination. This is further demonstrated by analyzing the emission property at room temperature.

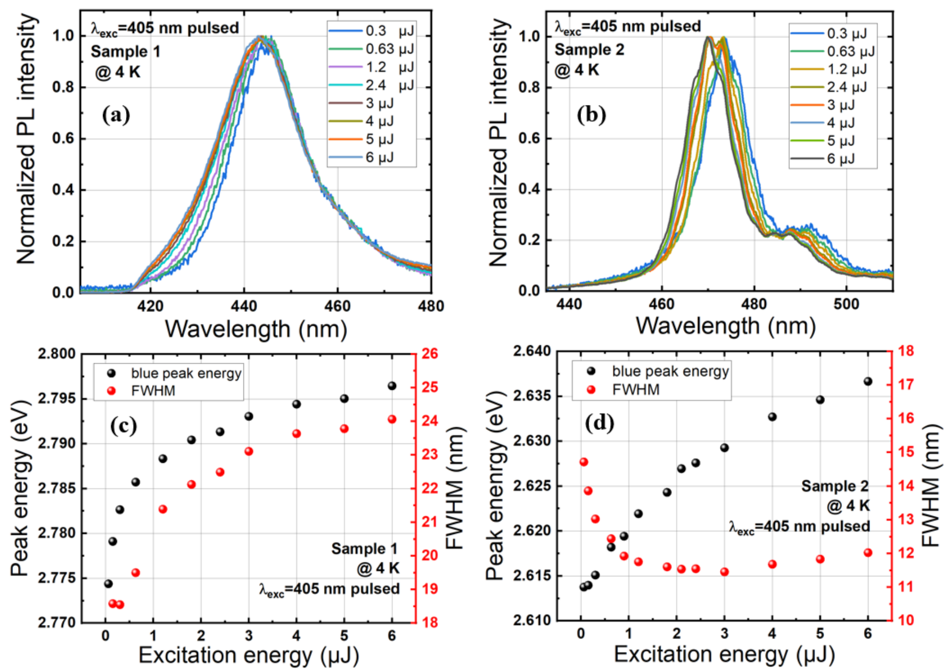

Fig. 2. Normalized blue peak PL spectra of Sample 1 (a) and Sample 2 (b) at different excitation energy (4 K). Emission peak energy and FWHM as functions of excitation energy for the pre-QW emission at 4 K, (c) Sample 1 and (d) Sample 2.

At 300 K, the non-radiative recombination centers due to defects will be activated and play a role in carriers recombination process. The relation between the integrated PL intensity of pre-QW emission and the excitation energy are shown in Fig. 3(a) and (b) at RT. The integrated PL intensity (I) as a function of the excitation energy (E) can be expressed by the following equation [22]:

$$\boldsymbol{I} \propto \boldsymbol{E}^{\boldsymbol{F}} \tag{1}$$

when F = 1, radiative recombination is dominated. As shown in Fig. 3, the F values are 0.893 and 1.035, respectively. The F value of Sample 2 is very close to 1, indicating the pre-QW emission of Sample 2 is dominated by radiation recombination at 300 K. Meanwhile, the IQE value can be calculated by the ratio of integrated PL intensities at 300 and 15 K [23–25]. The IQE of blue peak in Sample 1 is 54.3%, and that of Sample 2 is 88.3%, which is a good proof of the decrease in non-radiative recombination in Sample 2.

Next, the optical properties of the red QWs in two samples are analyzed and discussed. The excitation-energy-dependent normalized PL spectra of red peaks are shown in Fig. 4. The red peak of Sample 1 is characterized by a wider FWHM and a larger blue shift, demonstrating large In fluctuation, strong QCSE and band filling in the red QW. In comparison, the red peak of

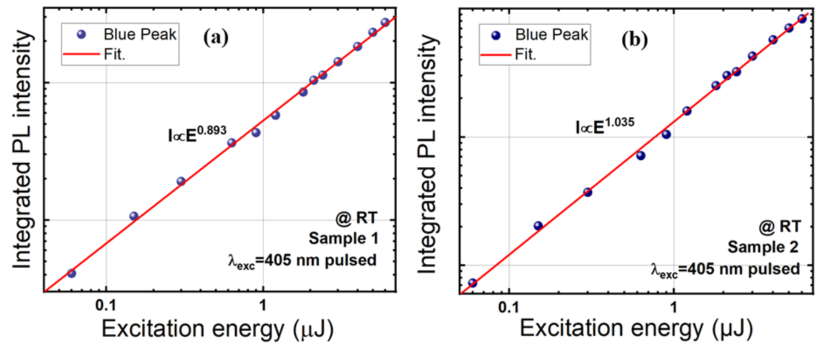

Fig. 3. Integrated PL intensity as a function of excitation energy for the pre-QW at 300 K, (a) Sample 1 and (b) Sample 2.

Sample 2 presents a narrower FWHM, a smaller blue shift and a broadening in short wavelength side, demonstrating less In fluctuation, less QCSE and pronounced band filling effect. In previous literatures [26,27], the QW with wider well layer existed a poor carrier confinement and serious QCSE, leading to a weaker PL intensity and a larger shift of peak wavelength. However, Sample 2 with 3.5-nm red QWs possesses a narrower FWHM, a stronger PL intensity and a small blue shift compared with Sample 1 with 2.5-nm red QWs. These results indicate that higher-In-content pre-QW can effectively alleviates the residual compressive stress from the underlayers. The higher-In-content pre-InGaN layer also plays a stretching role on the barrier layer of red QW, reducing the mismatch between strained GaN barrier and the red InGaN layer with even higher In content. The process of adjusting strain in red InGaN layers by the blue pre-QW is schematically shown in Fig. 5. The higher In uniformity and less QCSE lead to an increase in spatial overlap of electron and hole wave-functions and higher spontaneous recombination rate.

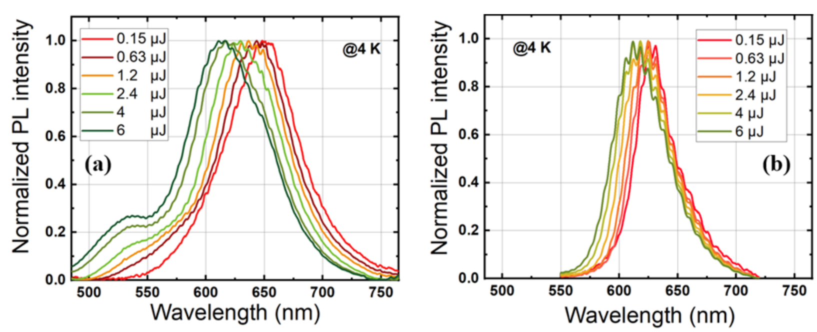

Fig. 4. Normalized red peak PL spectra of two samples at different excitation energy (4 K), (a) Sample 1 and (b) Sample 2.

By fitting curves, we obtain the FWHMs and emission energies of red QWs at different excitation energies, shown in Fig. 6. The red peak of Sample 1 possesses a wider FWHM (<89 nm) and a larger blue shift of peak energy (~100 meV), indicating the serious localized states effect caused by In fluctuation in the red QW. The blue shift of peak energy in Sample 2 is smaller (~40 meV), and the FWHM (<66 nm) is narrower, indicating a weak In fluctuation and shallower localized states effect. Compared with the PL intensity of two samples, it is found that the red QW of Sample 2 presents stronger radiative recombination. The decrease of residual stress, the high growth temperature (>20 °C) and the improvement of In-content homogeneity enhance the PL intensity and reduce the FWHM in the red QWs.

Optics EXPRESS

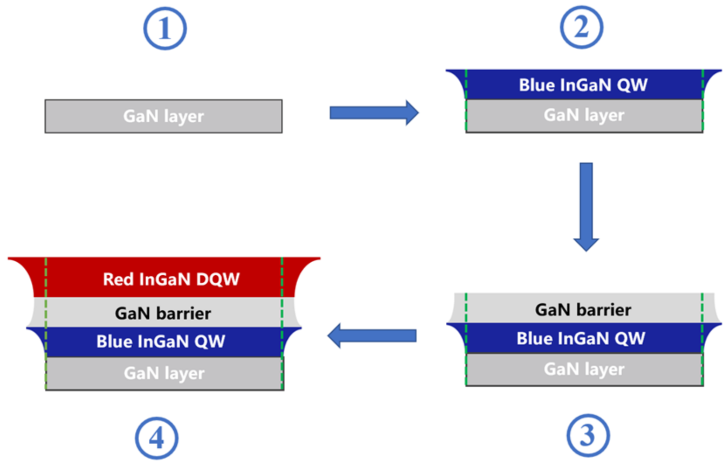

Fig. 5. The schematic of strain evolution in red InGaN layers by the blue pre-QW.

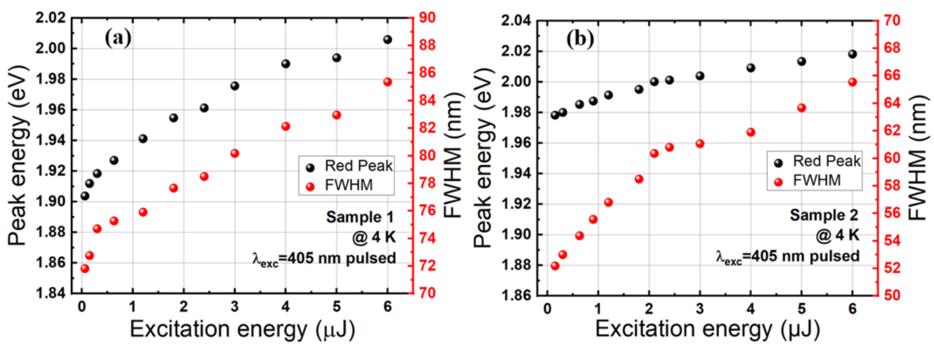

Fig. 6. Emission peak energy and FWHM as functions of excitation energy for red peak (4 K), (a) Sample 1 and (b) Sample 2.

In order to further investigate the optical characteristics of red QWs, the PL spectra of Samples 1 and 2 were investigated in the temperature range 15-300 K as shown in Fig. 7. The IQE values of red QWs for two samples are calculated [23–25]. The IQE of red peak in Samples 1 and 2 was found to be 13.5% and 20.5%, respectively. Sample 2 shows a higher value of IQE.

According to the PL characteristics of the samples, we proposed the model of the localized states in the red QW as shown in Fig. 8. Sample 1 possesses the serious In fluctuation and deep localized states in red QW, leading to a wider FWHM. In the deep localized state, the confinement of carrier is more serious, and the density of states is smaller, which affects the emission efficiency. The red QW of Sample 2 has a smaller In fluctuation and shallower localized states. The FWHM is narrower and the carriers are weakly localized, which increases the recombination probability of carriers, and then improves its luminescence intensity. This model can well explain the optical characteristics of red QW in two samples.

The model is demonstrated by TRPL measurement. The TRPL curves at the peak energy are fitted by one- and two-exponential functions as shown in Fig. 9. The equations are as follows [13,28]:

$$I(t) = \boldsymbol{B}_1 \times \exp(\frac{-t}{\boldsymbol{\tau}_1}) \tag{2}$$

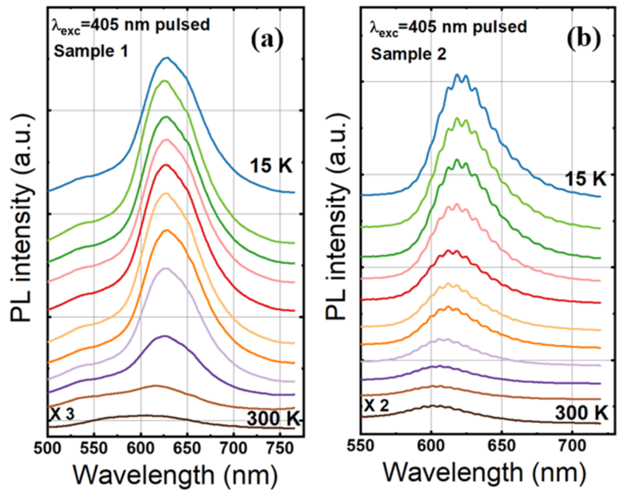

Fig. 7. The temperature-dependent PL spectra of red peak at 15-300 K, (a) Sample 1 and (b) Sample 2.

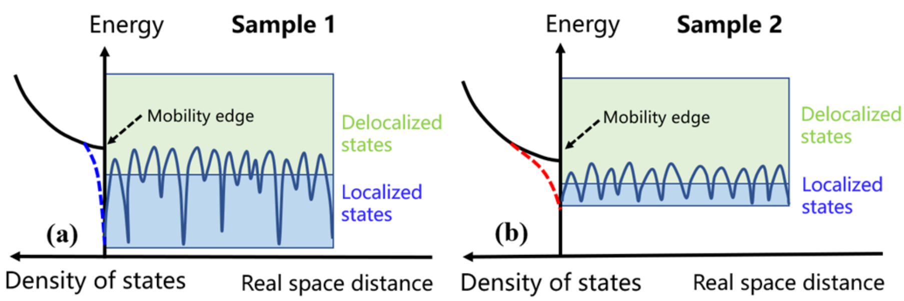

Fig. 8. The schematic of localized states model in red QWs of two samples.

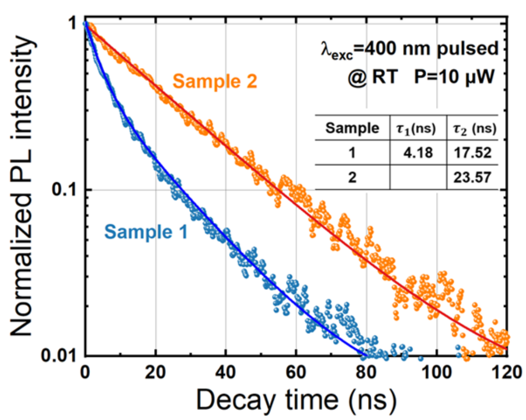

Fig. 9. TRPL curves and fitting results of red emission peak for two samples.

Optics EXPRESS

$$I(t) = \boldsymbol{B}_1 \times \exp(\frac{-t}{\tau_1}) + \boldsymbol{B}_2 \times \exp(\frac{-t}{\tau_2}) \tag{3}$$

where $I(t)$ is the PL intensity at time t. The parameters τ_1 and τ_2 are the fast and slow decays, respectively. The decay curve of red QW in Sample 1 is obviously a double-exponential function. The fast and slow decay times are 4.18 ns and 17.52 ns, respectively. This result indicates that the localized states in the red QWs of Sample 1 are more severe, resulting in the long-time transfer and recombination processes of photo-generated carrier. The decay curve of Sample 2 is a single-exponential function, obtained the decay time 23.57 ns. The carriers of red QW are recombination only, and there is no carrier transfer in Sample 2. At the same time, the shorter decay time of Sample 1 is attributed to the fact that more non-radiative recombination centers in red QWs are activated at room temperature. This result is consistent with the higher IQE value and stronger PL intensity of Sample 2. Based on the above discussion, the variation in growth conditions and related conclusions are summarized in the Table. 2.

Table 2. The conclusions and different parameters of two samples

Structure	Sample 2	Conclusions
$Al_{0.13}Ga_{0.87}N$ (barrier)	Lower growth rate	1) Longer annealing on the QW 2) Uniform In distribution in the QW
Blue QW (pre-well layer)	Lower growth temperature	Higher In content in the blue QW
Red QWs (active layers)	3.5 nm (wider width)	Larger carrier confinement potential
	Higher growth temperature	Quality up
	Higher growth rate	Uniform In distribution

4. Conclusion

In this work, we present the characterization of red InGaN/GaN MQWs epitaxial wafers. The optical properties of two red MQWs structures with different well widths are studied and compared. The results show that the higher-In-content pre-well layer alleviates the residual compressive stress, and reduces the mismatch between strained GaN barrier and the red InGaN layer with high In component. Therefore, the red QW with 3.5-nm well width possesses a weak QCSE, helping to improve the overlap of electron and hole wave functions and enhance the probability of recombination. Secondly, the high growth temperature (>20 °C) of the red QW improved the crystal quality, and finally the PL intensity and IQE of red QW are improved while the FWHM is reduced.

Funding. National Natural Science Foundation of China (62234011, U21A20493, 62104204); National Key Research and Development Program of China (2017YFE0131500).

Acknowledgments. The authors would like to thank Zhong-Ming Zheng, Lei-Ying Ying, Zhi-Wei Zheng and Hao Long of Xiamen University for support and useful discussions.

Disclosures. The authors declare no conflicts of interest.

Data availability. Data underlying the results presented in this paper are not publicly available at this time but may be obtained from the authors upon reasonable request.

References

1. Y. Narukawa, M. Ichikawa, D. Sanga, M. Sano, and T. Mukai, "White light emitting diodes with super-high luminous efficacy," J. Phys. D: Appl. Phys. **43**(35), 354002 (2010).
2. Q. Lv, J. Liu, C. Mo, J. Zhang, X. Wu, Q. Wu, and F. Jiang, "Realization of Highly Efficient InGaN Green LEDs with Sandwich-like Multiple Quantum Well Structure: Role of Enhanced Interwell Carrier Transport," ACS Photonics **6**(1), 130–138 (2019).
3. M. Broell, P. Sundgren, A. Rudolph, W. Schmid, A. Vogl, and M. Behringer, "New developments on high-efficiency infrared and InGaAlP light-emitting diodes at OSRAM Opto Semiconductors," Proc. SPIE **9003**, 90030L (2014).

4. S. N. Zhang, J. L. Zhang, J. D. Gao, X. L. Wang, C. D. Zheng, M. Zhang, X. M. Wu, L. Q. Xu, J. Ding, Z. J. Quan, and F. Y. Jiang, "Efficient emission of InGaN-based light-emitting diodes: Toward orange and red," Photonics Res. **8**(11), 1671–1675 (2020).
5. A. Koukitu, N. Takahashi, T. Taki, and H. Seki, "Thermodynamic analysis of the MOVPE growth of InAlN," J. Cryst. Growth **170**(1-4), 306–311 (1997).
6. M. Shimizu, Y. Kawaguchi, K. Hiramatsu, and N. Sawaki, "Metalorganic Vapor Phase Epitaxy of Thick InGaN on Sapphire Substrate," Jpn. J. Appl. Phys. **36**(6R), 3381 (1997).
7. Y. Yamashita, H. Tamura, N. Horio, H. Sato, K. Taniguchi, T. Chinone, S. Omori, and C. Funaoka, "Control of Emission Wavelength of GaInN Single Quantum Well, Light Emitting Diodes Grown by Metalorganic Chemical Vapor Deposition in a Split-Flow Reactor," Jpn. J. Appl. Phys. **42**(Part 1, No. 7A), 4197–4202 (2003).
8. D. Holec, P. M. F. J. Costa, M. J. Kappers, and C. J. Humphreys, "Critical thickness calculations for InGaN/GaN," J. Cryst. Growth **303**(1), 314–317 (2007).
9. S. S. Pasayat, C. Gupta, M. S. Wong, R. Ley, M. J. Gordon, S. P. DenBaars, S. Nakamura, S. Keller, and U. K. Mishra, "Demonstration of ultra-small (<10 µm) 632 nm red InGaN micro-LEDs with useful on-wafer external quantum efficiency (>0.2%) for mini-displays," Appl. Phys. Express **14**(1), 011004 (2021).
10. A. Dussaigne, P. L. Maitre, H. Haas, J. C. Pillet, F. Barbier, A. Grenier, N. Michit, A. Jannaud, R. Templier, D. Vaufrey, F. Rol, O. Ledoux, and D. Sotta, "Full InGaN red (625 nm) micro-LED (10 µm) demonstration on a relaxed pseudo-substrate," Appl. Phys. Express **14**(9), 092011 (2021).
11. P. P. Li, H. J. Li, H. J. Zhang, C. Lynsky, M. Iza, J. S. Speck, S. Nakamural, and S. P. DenBaars, "Size-independent peak external quantum efficiency (>2%) of InGaN red microlight-emitting diodes with an emission wavelength over 600 nm," Appl. Phys. Lett. **119**(8), 081102 (2021).
12. D. Iida, S. Lu, S. Hirahara, K. Niwa, S. Kamiyama, and K. Ohkawa, "Enhanced light output power of InGaN-based amber LEDs by strain-compensating AlN/AlGaN barriers," J. Cryst. Growth **448**, 105–108 (2016).
13. D. Iida, K. Niwa, S. Kamiyama, and K. Ohkawa, "Demonstration of InGaN-based orange LEDs with hybrid multiple-quantum-wells structure," Appl. Phys. Express **9**(11), 111003 (2016).
14. D. Iida, Z. Zhuang, P. Kirilenko, M. Velazquez-Rizo, M. A. Najmi, and K. Ohkawa, "633-nm InGaN-based red LEDs grown on thick underlying GaN layers with reduced in-plane residual stress," Appl. Phys. Lett. **116**(16), 162101 (2020).
15. P. Chan, V. Rienzi, N. Lim, H. M. Chang, M. Gordon, S. P. DenBaars, and S. Nakamura, "Demonstration of relaxed InGaN-based red LEDs grown with high active region temperature," Appl. Phys. Express **14**(10), 101002 (2021).
16. D. Iida, P. Kirilenko, M. Velazquez-Rizo, Z. Zhuang, M. A. Najmi, and K. Ohkawaa, "Demonstration of 621-nm-wavelength InGaN-based single-quantum-well LEDs with an external quantum efficiency of 4.3% at 10.1 A/cm^2," AIP Adv. **12**(6), 065125 (2022).
17. Y. M. Huang, C. Y. Peng, W. C. Miao, H. Chiang, T. Y. Lee, Y. H. Chang, K. J. Singh, D. Iida, R. Horng, C. W. Chow, C. C. Lin, K. Ohkawa, S. C. Chen, and H. C. Kuo, "High-efficiency InGaN red micro-LEDs for visible light communication," Photonics Res **10**(8), 1978 (2022).
18. X. Hou, S. S. Fan, H. Xu, D. Iida, Y. J. Liu, Y. Mei, G. E. Weng, S. Q. Chen, B. P. Zhang, and K. Ohkawa, "Optical properties of InGaN-based red multiple quantum wells," Appl. Phys. Lett. **120**(26), 261102 (2022).
19. D. Iida and K. Ohkawa, "Recent progress in red light-emitting diodes by III-nitride materials," Semicond. Sci. Technol. **37**(1), 013001 (2022).
20. G. E. Weng, J. Y. Yan, S. J. Chen, C. H. Zhao, H. B. Zhang, J. Tian, Y. J. Liu, X. B. Hu, J. H. Tao, S. Q. Chen, Z. Q. Zhu, H. Akiyama, and J. H. Chu, "Superiosr Single-Mode Lasing in Self-Assembly $CsPbX_3$ Microcavity over an Ultrawide Pumping Wavelength Range," Photonics Res. **1**, 54–65 (2020).
21. X. Hou, S. S. Fan, D. Iida, Y. Mei, B. P. Zhang, and K. Ohkawa, "Photoluminescence of InGaN-based red multiple quantum wells," Opt. Express **29**(19), 30237–30243 (2021).
22. Z. M. Zheng, Y. Mei, H. Long, H. Jason, S. P. Guo, Q. X. Li, L. Y. Ying, Z. W. Zheng, and B. P. Zhang, "AlGaN based deep ultraviolet vertical cavity surface emitting laser," IEEE Electron Device Lett. **42**(3), 375–378 (2021).
23. Z. Zhuang, D. Iida, and K. Ohkawa, "InGaN-based red light-emitting diodes: From traditional to micro-LEDs," Jpn. J. Appl. Phys. **61**(SA), SA0809 (2022).
24. Y. L. Lai, C. P. Liu, Y. H. Lin, T. H. Hsueh, R. M. Lin, D. Y. Lyu, Z. X. Peng, and T. Y. Lin, "Origins of efficient green light emission in phase-separated InGaN quantum wells," Nanotechnology **17**(15), 3734–3739 (2006).
25. R. Li, M. S. Xu, P. Wang, C. X. Wang, S. D. Qu, K. J. Shi, Y. H. Wei, X. G. Xu, and Z. W. Ji, "Combined effects of carrier scattering and Coulomb screening on photoluminescence in InGaN/GaN quantum well structure with high In content," Chin. Phys. B **30**(4), 047801 (2021).
26. J. Bai, T. Wang, and S. Sakai, "Influence of the quantum-well thickness on the radiative recombination of InGaN/GaN quantum well structures," J. Appl. Phys. **88**(8), 4729 (2000).
27. T. S. Ko, T. C. Lu, T. C. Wang, J. R. Chen, R. C. Gao, M. H. Lo, H. C. Kuo, S. C. Wang, and J. L. Shen, "Optical study of *a*-plane InGaN/GaN multiple quantum wells with different well widths grown by metal-organic chemical vapor deposition," J. Appl. Phys. **104**(9), 093106 (2008).
28. M. Pophristic, F. H. Long, C. Tran, R. F. Karlicek, Z. C. Feng, and I. T. Ferguson, "Time-resolved spectroscopy of $In_xGa_{1-x}N$/GaN multiple quantum wells at room temperature," Appl. Phys. Lett. **73**(6), 815–817 (1998).